Atmospheric
Chemistry
and Physics
Discussions

Open Access

EGU

1 **Direct radiative effect of carbonaceous aerosols from crop residue**

2 **burning during the summer harvest season in East China**

3 Huan Yao[1], Yu Song[1,*], Mingxu Liu[1], Tingting Xu[1], Pin Du[1], Jianfeng Li[1], Yusheng Wu[1],

4 Min Hu[1], Tong Zhu[1]

5 [1] State Key Joint Laboratory of Environmental Simulation and Pollution Control,

6 Department of Environmental Science, Peking University, Beijing, China

7 * Corresponding author: songyu@pku.edu.cn

8 **Abstract**

9 The East China experiences extensive crop residue burning in fields during harvest

10 seasons. The direct radiative effect (DRE) of carbonaceous aerosols from crop residue

11 burning in June 2013 in East China was investigated using the Weather Research and

12 Forecasting Model coupled with Chemistry (WRF-Chem). Absorption of organic aerosol

13 (OA) in the presence of brown carbon (BrC) was considered using the parameterization

14 of Saleh et al. (2014), in which the imaginary part of BrC refractive index was a function

15 of the ratio of the black carbon (BC) and OA and wavelengths. The carbonaceous

16 emissions from crop fires were estimated using the Moderate Resolution Imaging

17 Spectroradiometer (MODIS) fire radiative power products with a localized crop

18 burning-sourced BC-to-organic carbon (OC) ratio emission ratio of 0.27. The simulation

19 results were evaluated with in situ measurements of fine particle ($PM_{2.5}$) chemical

20 components and meteorological observations. The aerosol optical depths were

21 comparable with MODIS detections. The BC and OC peak concentrations reached 34.3

22 µg m^{-3} and 121.1 µg m^{-3}, of which the crop residue burning contributed 86% and 90%,

23 respectively. Correspondingly, the DREs of crop residue burning-sourced BC and BrC

24 (due to absorption) reached +20.16 W m^{-2} and +7.17 W m^{-2}, respectively. On average,

25 during the harvest season, crop residue burning introduced a DRE of +0.39 W m^{-2}

26 throughout East China. We found that BrC absorption and BC introduced significant

27 positive DREs, +0.85 W m^{-2} and +1.05 W m^{-2}, respectively. The BrC DRE due to

28 scattering was stronger (-1.1 W m^{-2}) than its DRE due to absorption. The sensitivity test

29 showed that the BrC DRE strongly depended on the absorptivity and BC-to-OA ratio

30 emission ratio from crop residue burning, and the volume mixing treatment could result

31 in a higher positive DRE compared to the core/shell treatment.

32 **Keywords:** Carbonaceous aerosols; direct radiative effect; crop residue burning; East

33 China

34 **1. Introduction**

35   Carbonaceous aerosols emitted from biomass burning contribute 42% and 74% of

36 global black carbon (BC) and organic carbon (OC) emissions, respectively (Bond, 2004),

37 playing an important role in the radiation budget system (Chung et al., 2012; Hobbs et al.,

38 1997; Jacobson, 2014). The Intergovernmental Panel on Climate Change (IPCC) Fifth

39 Assessment Report stated that BC from biomass burning introduced a global mean direct

40 radiative forcing (DRF) of approximately +0.2 (+0.03 to +0.4) W m^{-2}, while that of

41 organic aerosol (OA) from biomass burning was about the same magnitude with the

42 opposite sign (Bond et al., 2013; Stocker, 2014). DRF is a measure of the change in

Atmospheric
Chemistry
and Physics
Discussions

Open Access

EGU

43　direct radiative effect (DRE) relative to preindustrial conditions, defined as year 1750 by

44　the IPCC. Precise computing of short term DRE caused by carbonaceous aerosols is

45　primary and essential to aerosol DRF estimation, avoiding the large uncertainties in

46　estimations of preindustrial carbonaceous aerosol emissions (Bond et al., 2013). DRE,

47　namely the radiative effect due to aerosol–radiation interactions, could also be a more

48　exhaustive gauge for comparisons between models and observations (Heald et al., 2014).

49　　　Aside from the established sunlight-absorbing BC from imperfect combustion

50　sources (Chang et al., 1982), the other co-emitted organic carbonaceous aerosol was

51　found to have an absorptive component closely linked to biomass burning (Kirchstetter et

52　al., 2004; Lack et al., 2012), commonly termed brown carbon (BrC) (Andreae, 1995),

53　which contributed a positive mean radiative forcing of +0.1 W m^{-2} to +0.25 W m^{-2} by

54　absorption globally (Feng et al., 2013). BrC radiation absorption is characterized by a

55　strong dependence on wavelength, increasing sharply from the short visible to the

56　ultraviolet ranges (Andreae and Gelencsér, 2006; Bond, 2001). The light absorption of

57　BrC from different sources is also highly variable; and for biomass burning, the

58　temperature of the combustion process, moisture content, and fuel type can be factors,

59　thus complicating the treatment of BrC in models (Laskin et al., 2015). Therefore, studies

60　using constant optical parameters of BrC for climate forcing calculations would have

61　significant uncertainties (Feng et al., 2013; Wang et al., 2014). Recently, Saleh et al.

62　(2014) proposed that the absorptivity of BrC from biomass burning, both fresh and aged,

63　could be parameterized as a function of the BC-to-OA ratio. This parameterization has

64　been used to simulate the DRE of BrC from biomass or biofuel burning emissions

Atmospheric
Chemistry
and Physics
Discussions

Open Access

EGU

65   globally in several studies (Kodros et al., 2016; Kodros et al., 2015; Saleh et al., 2015).

66   Off-line models with discrepancies in physical parameterizations between chemical and

67   meteorological simulations could also produce some errors (Gu et al., 2006).

68   As a large agricultural country, China emits approximately 97 Gg BC and 463 Gg OC

69   annually from crop residue burning in fields, mainly concentrated during the harvest

70   season in East China (Lu et al., 2011; Zhang et al., 2008).The previous emission

71   estimations were primarily derived from provincial statistical data with coarse spatial and

72   temporal resolutions. Only one study focused on the DRE of crop burning-sourced

73   carbonaceous aerosol over China and thus the DRE uncertainties could be very large,

74   especially during harvest season in East China (Li et al., 2016).

75   In this study, the DRE of carbonaceous aerosol from crop residue burning in East

76   China was quantified using the online Weather Research and Forecasting Model coupled

77   with Chemistry (WRF-Chem), with high-resolution carbonaceous aerosols emissions

78   from crop fires. The BrC absorptivity and its variation with wavelength and BC-to-OA

79   ratio were considered. The simulation was conducted for the harvest season in June 2013.

80   **2. Methods and Data**

81   2.1. Model Configuration

82   The online coupled meteorology-chemistry model, WRF-Chem version 3.6.1 (Grell

83   et al., 2005), was used. Double-nested domains centered at 36.5° N, 115.52° E, were set

84   with the coarse domain divided into 51 × 59 grid cells of 75-km horizontal resolution and

85   the fine domain divided into 48 × 63 grid cells of 25-km resolution (Fig. 1). The 25

Atmospheric
Chemistry
and Physics
Discussions

Open Access

86   vertical layers from the ground level to the top pressure of 50 hPa were used for all grids.

87   The Yonsei University (YSU) boundary layer vertical diffusion scheme (Hong and

88   Dudhia, 2003) was adopted. The global atmospheric reanalysis data ERA-Interim

89   produced by the European Centre for Medium-Range Weather Forecasts (ECMWF) was

90   used as the initial meteorological fields and boundary conditions with 3-hourly surface

91   parameters and 6-hourly upper-air parameters (Dee et al., 2011). The meteorology fields

92   were initialized at the start of each model run, which covered 36 h with the first 12 h as a

93   spinup. The simulated time covered the entire month of June, which was the local harvest

94   season of the main crop (wheat), and the model was conducted from 26 May to minimize

95   the impact from initial conditions. The domain settings and configuration options are

96   presented in Table 1.

97   For gas-phase chemistry, we chose the Model for Ozone and Related chemical

98   Tracers version 4 (MOZART-4) mechanism (Emmons et al., 2010) extended with clearer

99   aromatic compounds and monoterpenes treatments (Knote et al., 2014). The aerosol

100   processes, such as coagulation and thermodynamic equilibrium, were treated using the

101   Model for Simulating Aerosol Interactions and Chemistry (MOSAIC) scheme (Zaveri et

102   al., 2008), in which four discrete size bins were distinguished by dry physical particle

103   diameters (0.039–0.156, 0.156–0.625, 0.625–2.5, and 2.5–10.0 μm). A simplified

104   parameterization for secondary organic aerosol (SOA) formation was also incorporated

105   into the model by using CO from anthropogenic or biomass burning sources as a proxy

106   for SOA precursors based on the observed ratio between SOA and CO in polluted regions

107   (Hodzic et al., 2010). In WRF-Chem, aqueous phase chemistry was closely associated

Atmospheric
Chemistry
and Physics
Discussions

Open Access

EGU

108   with indirect effect modeling and was not included in this study.

109   The DRE estimates were derived from the instantaneous shortwave flux changes

110   between different scenarios (further explained in section 2.4) at top of atmosphere (TOA)

111   for average cloudy skies (i.e., all-sky conditions), with only direct radiative feedback

112   considered. Taking advantage of the multiple scattering handling capability and taking

113   both computing speed and accuracy into consideration, the rapid radiative transfer model

114   (RRTMG) (Mlawer et al., 1997) was selected to simulate shortwave flux change. We

115   ignored the radiative effect of gaseous materials emitted by crop residue burning and

116   focused on the shortwave aerosol DRE.

117   Aerosol optical properties, including absorption efficiency, scattering efficiency, and

118   the asymmetry parameter, are necessary for aerosol radiative transfer calculations. In this

119   study, these three parameters were computed by the shell/core Mie theory for each bin

120   (Ackerman and Toon, 1981) and then determined by summation over all size bins (Fast

121   et al., 2006). The spherical shell/core configuration was selected for the calculations of

122   aerosol optical properties, in which the BC core is assumed to be coated with a

123   homogeneously mixed shell of other species. For each bin, the complex refractive index

124   of the shell was derived by volume averaging that of every shell species (Barnard et al.,

125   2010), except for the imaginary refractive index of OA, which was zero by default. In

126   this study, we adopted the Saleh et al. (2014) parameterization to calculate the BrC

127   absorptivity, which formulating the imaginary part of OA's refractive index k_{OA} with the

128   ratio of BC and OA from biomass burning as following:

Atmospheric
Chemistry
and Physics
Discussions

Open Access

EGU

129
$$k_{OA,550} = 0.016 \log_{10}\left(\frac{BC}{OA}\right) + 0.04 \qquad (1)$$

130
$$\omega \ = \ \frac{0.21}{\left(\frac{BC}{OA}+0.07\right)} \qquad (2)$$

131
$$k_{OA} = k_{OA,550}\left(\frac{550}{\lambda}\right)^{\omega} \qquad (3)$$

132   The $k_{OA,\,550}$ is the imaginary part of OA's refractive index at wavelength (λ) of 550nm

133   and ω is the wavelength dependence of k_{OA}.

134   2.2. Emission Inventory

135   The crop residue burning emissions were derived based on fire radiative power (FRP)

136   from the Moderate Resolution Imaging Spectroradiometer (MODIS) products (Liu et al.,

137   2015). The FRP method could reduce emission uncertainties when compared to

138   traditional methods, in which multi-parameters that depend on local agricultural practices

139   were used. Moreover, the crop residue fires were often small and not captured by

140   MODIS burned area products (Roy et al., 2008). The emissions based on the FRP method

141   had 1-km and daily resolutions.

142   The BC and OC emission factors from crop fires in this study (1.98 g/kg and 0.54

143   g/kg, respectively) were set specifically for the winter wheat residue burning in East

144   China. It was averaged using published emission factors from winter wheat combustion

145   simulating experiments in the field or laboratory (Hays et al., 2005; Li et al., 2007;

146   Dhammapala et al., 2007; Turn et al., 1997). The BC-to-OC ratio from crop burning was

147   0.27, falling within the range of 0.20–0.32 observed during harvest seasons in East China

148   (Li et al., 2014; Yamaji et al., 2010; Yang et al., 2008).

Atmospheric
Chemistry
and Physics
Discussions

Open Access

EGU

149   The Multi-resolution Emission Inventory for China (MEIC, see www.meicmodel.org)

150   database was applied for China, and the Mosaic Asian Anthropogenic Emission

151   Inventory (MIX, see http://www.meicmodel.org/dataset-mix.html) database (Li et al.,

152   2015) was applied for the surrounding countries, including power plant, industrial,

153   residential, and vehicle emissions.

154   2.3. In Situ Measurements and Other Data

155   Fine particle ($PM_{2.5}$) chemical components were sampled and analyzed from May 30

156   to June 27, 2013 at the site (33°54′37″ N, 116°45′46″ E) in Suixi, Anhui Province, China,

157   close to vast stretches of wheat fields, the nearest of which was only 1 km away. There

158   were two sampling periods each day: from approximately 7:40 (GMT+8.0) to 18:00 and

159   from 18:40 to 7:00 the next morning. BC and OA were assessed by a thermal/optical

160   carbon analyzer (Sunset Laboratory, Tigard, OR, USA) with quartz-fiber filters. More

161   complete detail on sampling and analysis can be found in Li et al. (2014).

162   The MODIS Level-2 Atmospheric Aerosol Product (04_L2) data (Collection 6), at a

163   1-km daily resolution for June 2013, was used to evaluate the aerosol optical depth

164   (AOD) simulations, with the Deep Blue algorithms (Hsu et al., 2006) integrated with the

165   existing MODIS algorithm to retrieve AOD over the entire land area, including both dark

166   and bright surfaces.

167   2.4. Numerical Experiments

168   Seven parallel simulations were conducted to investigate the DRE of carbonaceous

169   aerosols from crop residue burning, as well as the effects of mixing state and BrC

Atmospheric
Chemistry
and Physics
Discussions

170   absorption (Table 2). The default simulation, namely the BASE simulation, covered the

171   whole emissions and presumed BC cores coated by shells of other well-mixed aerosols.

172   The OA absorption was parameterized based on Saleh et al. (2014). The crop residue

173   burning DRE was estimated by the difference between the BASE and NOCB runs. To

174   compute the DRE from BC and OA from crop residue burning (i.e. NOBCCB and

175   NOOACB, respectively), we conducted two more parallel simulations without the

176   corresponding BC and OA emissions. Another simulation was performed by setting the

177   imaginary part of the OA refractive index to zero (NOBRC), to study the DRE values

178   caused by OA absorption.

179   **3. Results and Discussion**

180   3.1. Model Evaluation

181   The meteorological results in BASE simulation were evaluated by comparison with

182   the land-based station data in East China. Considering the extension of the inner domain

183   and the simulation period of June 2013, we chose the temperature and relative humidity at

184   2 m above ground surface (T2 and RH2, respectively) and the wind speed and direction at

185   10 m above ground (WS10 and WD10) from 221 matched stations. Statistical indices

186   (Table 3), including mean bias (MB), root-mean-square error (RMSE), fractional bias (FB),

187   fractional error (FE), and index of agreement (IOA), indicated that the model

188   well-simulated both temporal variations and spatial distributions of the four

189   meteorological items. The model well-reproduced the T2 and RH2, with IOAs of 0.92 and

190   0.87, respectively. The statistical indices of T2 had slightly better coincidence than those

Atmospheric
Chemistry
and Physics
Discussions

Open Access

191   of RH2, with the RMSE of RH2 reaching 13.93. There was a small underestimation

192   (−0.69%) of RH2, while WS10 was slightly overstimated (0.99 m/s). At three typical sites

193   (Fuyang, Yanzhou, and Xuzhou) corresponding to the three main districts affected by crop

194   fire (mentioned below), the model well captured the general temporal trends of T2 and

195   RH2, although the RH2 was slightly underestimated (Fig. S1), which might lead to small

196   differences in certain aerosol physical properties (Chapman et al., 2009; Xia et al., 2007).

197   In general, the simulation results were comparable to the meteorological observations.

198   The temporal variation of fire counts detected by MODIS in East China in June 2013

199   is shown in Fig. 2a. Approximately 97% of the fire counts occurred from 1–21 June, while

200   the fire counts decreased to < 200 per day after 21 Jun. Throughout the rest of this study,

201   we focus on the summer harvest from 1–21 June. The districts most affected by crop

202   residue fire were the southeastern Henan and central Anhui provinces from 1–8 June, and

203   then the northern Anhui province from 9–16 June, with most of the North China Plain

204   involved (Fig. 2b). Then, crop fires mainly occurred in the northern Jiangsu and eastern

205   Shandong provinces from 17–21 June, with diminishing fire counts. It is worth noting that

206   the longitude and latitude of the fire area gradually increased over time in three phases,

207   corresponding to the harvest time regulation, which was from inland to coastland and from

208   the south to the north, tightly tied to the summer air temperature differences between the

209   marine and terrestrial climate and low and high latitude, respectively.

210   The carbonaceous aerosols concentrations were well-reproduced when compared to

211   the measurements in Suixi (Fig. 3). BC and OC concentrations showed similar trends that

212   fluctuated smoothly with values < 10 μg m^{-3} and 20 μg m^{-3}, respectively, and then the

Atmospheric
Chemistry
and Physics
Discussions

Open Access

EGU

213   concentrations began to increase on the night of 12 June, and reached a peak on the night

214   of 14 June night, with mean values of 34.3 $\mu g\ m^{-3}$ and 121.1 $\mu g\ m^{-3}$, respectively. The

215   peak value of OC was ~3−4 times that of BC, close to the BC-to-OC ratio of crop residue

216   burning emissions (0.27, in section 2.2), also indicating that the dominant source of

217   carbonaceous aerosols pollution was local biomass burning. During the severely polluted

218   period from 12–17 June, wheat residue burning contributed 68% and 73% of the BC and

219   OC concentrations, respectively, corresponding to the Positive Matrix Factorization results

220   (74.5% and 75.8%, respectively) in Li et al. (2014). The time variations of ammonium,

221   sulfate, and nitrate in $PM_{2.5}$ were also well-reproduced and had more fluctuation than that

222   of carbonaceous aerosols, indicating weaker correlation with the crop fires (Fig. S2).

223   The Suixi site was almost unaffected by the intensive fire counts in southeastern

224   Henan and central Anhui from 1–8 June, owing to the prevailing southeast wind, which

225   brought the pollutants to Henan, Shanxi, and northern Hebei Province (Fig. 4a). The peak

226   values of carbonaceous aerosols at the Suixi site were centralized around 12–16 June,

227   corresponding to the high fire counts in Northern Anhui during this period (Fig. 2). Most

228   of the North China Plain witnessed more than 15 $\mu g\ m^{-3}$ BC and 30 $\mu g\ m^{-3}$ OC due to the

229   local crop residue burning as well as the pollutants carried by the south wind. After 17

230   June, the main burning area moved east to the northern part of Jiangsu province, effecting

231   Shandong province and having less influence in Suixi. The main carbonaceous aerosols

232   polluted area during the summer harvest, with > 90% of the mass concentration

233   contributed by crop residue burning, also moved from south to north and from inland to

234   coastal areas (Fig. 4), corresponding to the fire counts distribution. Carbonaceous aerosols

Atmospheric
Chemistry
and Physics
Discussions

Open Access

EGU

235   increased rapidly in the evening at around 19:00–20:00 and reached peak values at dawn

236   (5:00–6:00), because of the relatively looser management of crop burning and weaker

237   boundary layer mixing at nighttime. After sunrise, the concentrations gradually decreased

238   as the fires slowly extinguished and the surface inversion coupled to layers aloft enhanced

239   vertical mixing (Cao et al., 2009).

240   The 550-nm AOD detected by MODIS was well-reproduced by WRF-Chem (Fig. 5a

241   and 5b), showing high values (above 1) in the North China Plain and Jinagsu, consistent

242   with the MODIS agricultural fire counts distribution during the summer harvest in Fig. 2.

243   Higher AODs in megacities, including Beijing, Shanghai, and Tianjin, might be

244   attributable to the increased sulfate and ammonium concentrations and scattering in

245   summer (Huang et al., 2015). We used linear interpolation between AOD at 400 nm and

246   600 nm to retrieve the AOD at 550 nm, as aerosol optical properties were computed only

247   at four wavelengths in the model (Nordmann et al., 2014). The MODIS AOD data around

248   23 sites were matched with the simulated AOD by hour, showing a normalized mean

249   deviation (NMD) of −16.1% and a correlation coefficient (R) of 0.52 (Fig. S3). This small

250   underestimation might be partly caused by the underestimation of the summer RH (Yoon

251   and Kim, 2006). Several studies have also noted that the MODIS retrieval AOD showed

252   high bias in ground-based measurements such as the Aerosol Robotic Network data

253   (Huang et al., 2015; Myhre et al., 2009; Zhao et al., 2013).

254   Aerosol absorption optical depth (AAOD) is an interactional outcome of three out of

255   the four factors that determine aerosol DRF (Bond et al., 2013; Schulz et al., 2006).

256   Similar patterns can be seen between the spatial distribution of 550-nm AAOD and the

257   carbonaceous aerosols concentration during the summer harvest (Fig. 5c and 5d),

258   especially at the junction of Henan, Anhui, Jiangsu, and Shandong. The short atmospheric

259   lifetimes of BC and BrC determined that the surface concentration was more restricted by

260   the map of emissions (Bond et al., 2013; Laskin et al., 2015; Zhuang et al., 2011), so the

261   serious pollution of carbonaceous aerosols and the higher AAOD might be traced from

262   local crop burning emissions. It is worth noting that we treat all-source OA as BrC, thus

263   amplifying the AAOD around the megacities of Beijing and Tianjin.

264   3.2. Direct Radiative Effect of Crop Residue Burning

265   Estimated by the difference between the BASE and NOCB simulations, a mean DRE

266   of +0.39 W m^{-2} was introduced by crop residue burning at TOA in East China during the

267   summer harvest (Table 4), much higher than the previous open biomass burning DRE

268   estimation. The carbonaceous aerosols emitted from crop residue burning were the

269   dominant contributors to the DRE, including the climate warming agent BC and the

270   traditional cooling agent OA. Due to the lower BC-to-OA ratio compared to fossil fuel

271   and indoor biomass combustion, open biomass burning was previously simulated to

272   produce a cooling-to-neutral DRE (Abel et al., 2005; Chung et al., 2012; Myhre et al.,

273   2013). The incorporation of the BrC absorptivity scheme in this study might have led to

274   the positive crop residue burning DRE (Feng et al., 2013).

275   The DRE of BC from crop residue burning was calculated to be +1.05 W m^{-2} at TOA

276   during the summer harvest based on the difference between the BASE and NOBCCB

277   simulations. This is higher than the DRE estimation from biomass burning BC (+0.1 W

Atmospheric
Chemistry
and Physics
Discussions

Open Access

EGU

278   m^{-2} to +0.5 W m^{-2}) in East China for the summer of 2010 by Li et al. (2016), which used

279   the offline model with a coarse resolution. The emission inventories they used might

280   underestimate the BC emission from open biomass burning, especially during the harvest

281   season or in the burning zone, due to the traditional estimation methods and spatial

282   allocation rules (Lu et al., 2011). The external mixing state that they assumed would also

283   result in a lower and less accurate DRE than the core/shell treatment (Jacobson, 2001).

284   After dividing the DRE of BC from crop residue burning by the corresponding source

285   contribution to the BC mass concentration (13.5%, Table 5), our all-source BC DRE

286   estimate at TOA for the summer harvest of +7.8 W m^{-2} was higher than the national

287   all-sky anthropogenic BC DRE for the summer of 2006 (+5 W m^{-2}) (Huang et al., 2015)

288   and in the range of the BC DRE in East China for the summer of 2008 (+5 W m^{-2} to +15

289   W m^{-2}) (Gao et al., 2014). It was worth noting that these previous studies neglected the

290   crop residue burning emissions and adopted the volume mixing treatment, which would

291   definitely overestimate the BC DRE. So the missing of crop residue burning could cause

292   an underestimation of 7%–17% in anthropogenic BC DRE during the summer harvest.

293   Normalized DRE, defined by (Boucher and Anderson, 1995) (and first used in (Feichter

294   et al., 1997)) as the ratio of the forcing to the aerosol mass burden, was calculated to

295   isolate differences in the aerosol column burden from the differences in all other model

296   processes that lead to carbonaceous aerosols radiative forcing (Bond et al., 2013).

297   Normalized DRE with respect to the BC burden from crop residue burning was

298   +1,109.72 W g^{-1} (Table 5), fell within the existing estimated global normalized DRF

299   ranges of +870 W g^{-1} to +2730 W g^{-1} (Bond et al., 2013; Ramanathan and Carmichael,

Atmospheric
Chemistry
and Physics
Discussions

300   2008; Schulz et al., 2006).

301   By subtracting the TOA shortwave flux of NOOACB from that of BASE, we

302   obtained an OA DRE from crop residue burning of –0.25 W m^{-2} in East China. The

303   normalized DRE of OA from crop residue burning, –57.17 W g^{-1} (Table 5), was also

304   comparable to the existing estimates of −24 W g^{-1} to −198 W g^{-1} (Bond et al., 2013;

305   Ramanathan and Carmichael, 2008; Schulz et al., 2006). The DRE of OA from crop

306   residue burning, calculated by the shortwave flux differences between the BASE and

307   NOOACB simulations, was a combination of the positive BrC DRE (+0.85 W m^{-2}) due

308   to absorption and the negative DRE (−1.1 W m^{-2}) due to scattering. The former was

309   calculated by multiplying the total OA DRE from absorption (the shortwave flux

310   differences between the BASE and NOBRC simulations) by the crop residue burning

311   contribution to the total OA mass concentration of 30.3% (Table 5), which was in

312   agreement with the previous observed range of 24%– 67.5% at sites in East China (Fu et

313   al., 2012; Li et al., 2014). This was above the ranges of both the global annual mean BrC

314   DRE from absorption, of +0.04 to +0.57 W m^{-2} (Feng et al., 2013; Saleh et al., 2015;

315   Wang et al., 2014), and the BrC DRE in East Asia for the spring of 2011, of +0.1 to +0.2

316   W m^{-2} (Park et al., 2010). The BrC DRE from crop residue burning accounted for 81% of

317   the corresponding BC DRE, higher than the previous estimation range of 27%–70% (Lin

318   et al., 2014), indicating that BrC could be a dominant light-absorbing aerosol during the

319   summer harvest in East China.

320   Figure 6 illustrates that the high values of BC DRE (above +3.0 W m^{-2}) and BrC

321   DRE due to absorption (above +1.5 W m^{-2}) during the summer harvest mainly appeared

Atmospheric
Chemistry
and Physics
Discussions

322   in the western Shandong, eastern Henan province, northern Anhui and northern Jiangsu

323   Provinces, similar to the spatial features of carbonaceous aerosol mass (Fig. 5d). The

324   hotspot was in the north of the intensive crop fire-affected area (Fig. 2b), as the dominant

325   southeastern wind in June transported the denser carbonaceous aerosols to the north

326   (section 3.1). With the carbonaceous aerosols mass concentration exceeding 35 µg m^{-3},

327   the southeastern Henan and northern Jiangsu had the highest BC DRE above +5.0 W m^{-2}

328   and BrC DRE above +5.0 W m^{-2} in our domain. The local DRE in the burning districts

329   during the crop residue burning periods could be higher than spatiotemporally averaged

330   estimates. Taking the Suixi site as an example, the mean crop residue burning

331   contributions to ambient BC and OA during the highest peaks (14–15 June) were 86%

332   and 90%, respectively. The corresponding mean DREs of crop residue burning-sourced

333   BC and BrC due to absorption reached +20.16 W m^{-2} and +7.17 W m^{-2}, respectively.

334   3.3 Uncertainty

335   The DRE of carbonaceous aerosols were strongly dependent on the optical properties,

336   the uncertainties of which came from various factors, including complex refractive

337   indices, mixing state and the morphologies of the particles. Since this study was the first

338   attempt to use the BrC absorptivity parameterization of Saleh et al. (2014) in online

339   model, sensitivity experiments were conducted to investigate the response of BrC DRE

340   to the changes in the imaginary part of OA's refractive index (k_{OA}) and the key parameter,

341   namely the BC-to-OC emission ratio from crop residue burning. As the k_{OA} was raised by

342   30% and 50%, the DRE of this source BRC due to absorption increased to +1.05 W m^{-2}

343   and +1.22 W m^{-2} (Table S2). This DRE value was estimated to be +0.96 W m^{-2} and

344   +0.81 W m^{-2} (Table S2), when BC-to-OA ratio was set to 0.18 (Li et al., 2007) and 0.42

345   (Hays et al., 2005), respectively, with the OA emission factor from crop residue burning

346   in consistent with the standard simulation. The sensitivity test of BC-to-OC ratio could

347   account for the uncertainties introduced by variable residue burning conditions and OA

348   volatility (Kodros et al., 2015). Efforts are still needed to update the BC-to-OC ratio

349   localized ratio observation in China. These results indicated that the k_{OA} and the

350   BC-to-OC emission ratio were critical for estimating BrC DRE. More details about

351   sensitivity test were presented in Table S1.

352   The sensitivity of BC mixing state to crop residue burning DRE was also tested by

353   changing the standard core/shell mixing to volume mixing, which assumed the particles

354   have a volume-averaged absorptivity and could lead to a higher absorption efficiency and

355   higher absorption coefficients than the former (Jacobson, 2000). In the volume mixing

356   treatment, crop residue burning was simulated to produce a mean DRE of +0.54 W m^{-2}

357   during the summer harvest (Table S2) The single-distribution core/shell assumption was

358   believed to be a better approximation of BC DRE (Bauer et al., 2013; Jacobson, 2001)

359   and more coated particles were observed in biomass burning aerosol (Schwarz et al.,

360   2008), so the widely-used volume mixing assumption could introduce an obvious DRE

361   discrepancy. The realistic carbonaceous aerosol mixing conditions are much more

362   various and complicated in time and space. For example, Peng et al. (2016) recently

363   reported that BC morphology varied from fractal particles to compact particles during

364   atmospheric aging, and BC in the two distinct stages revealed quite different absorption

365   characteristics and climatic effects. Therefore, the invariant core/shell assumption during

Atmospheric
Chemistry
and Physics
Discussions

Open Access

EGU

366   aging that we applied might overestimate the DRE of freshly emitted BC. This spherical

367   core/shell assumption might also amplify the absorption in cases in which the BC core

368   position is non-central (Adachi et al., 2010). The various moisture contents, as well as the

369   temperature conditions, also complicate the mixing state of carbonaceous aerosols and

370   the fraction and light absorptivity of BrC (Liu et al., 2013; Zhang et al., 2013). Moreover,

371   the lack of consideration of atmospheric processing of BrC, such as photobleaching

372   (Laskin et al., 2015), and the potential addition of nitrate groups (Jacobson, 1999), leads

373   to further uncertainties.

374   The high-resolution emission inventory based on the MODIS FRP used here may

375   add uncertainties to the carbonaceous aerosols mass concentrations and size distribution,

376   due to uncertainties arising from the MODIS detection resolution, FRP values, and the

377   per-fire-pixel Fire Radiative Energy (FRE) calculating method (Liu et al., 2015). The

378   simplified SOA formation scheme used in this study would also bring in uncertainties to

379   the OA concentration.

4. Conclusion

381   The DRE of carbonaceous aerosols from crop residue burning in June 2013 in

382   Eastern China was investigated using WRF-Chem. The BrC effective absorptivity

383   parameterization proposed by Saleh et al. (2014) was used. The carbonaceous aerosols

384   emissions from crop fires were estimated based on the MODIS FRP products, with the

385   localized BC-to-OC ratio from crop burning of 0.27. In situ observations conducted in

386   Suixi, Anhui Province, during the corresponding period were utilized to evaluate the

387   simulation. The WRF-Chem results well-captured the variation of carbonaceous aerosol

388   concentrations, showing peak pollution during the period from 12–17 June. The BC and

389   OC peak concentrations reached 34.3 μg m^{-3} and 121.1 μg m^{-3}, of which the crop residue

390   burning contributed 86% and 90%, respectively. The simulation results also

391   well-reproduced the temperature and relative humidity from ground-based observations

392   and MODIS-detected AODs, although there was a slight overestimation of wind speed.

393   During the summer harvest in East China (1–21 June), similar patterns were found

394   among simulated AAOD, fire counts detected by MODIS, and carbonaceous aerosols

395   concentrations, with higher values in the junction of Shandong, Henan, Anhui, and

396   Jiangsu provinces, confirming that the crop residue burning was the dominant cause for

397   the high AAOD.

398   The DREs of crop residue burning-sourced BC and BrC due to absorption reached

399   +20.16 W m^{-2} and +7.17 W m^{-2} in Suixi. On average, during the concentrated harvest,

400   crop residue burning introduced a DRE of +0.39 W m^{-2} throughout East China,

401   indicating that taking absorptive BrC into consideration caused the crop residue burning

402   DRE to become positive. The higher BC DRE (above +3.0 W m^{-2}) and BrC DRE due to

403   absorption (above +1.5 W m^{-2}) from crop residue burning during the concentrated

404   harvest mainly occurred in the North China Plain. BrC from crop residue burning as the

405   minor absorptive component brought about a significant positive DRE (+0.85 W m^{-2}),

406   accounting for 81% of the corresponding BC DRE (+1.05 W m^{-2}). The scattering

407   property of OA from crop residue burning was stronger (−1.1 W m^{-2}) than the absorptive

408   property, so the OA DRE was negative −0.25 W m^{-2}. The aerosol–radiation interaction

409 due to carbonaceous aerosols from crop residue burning in the summer harvest might

410 bring further effects on planetary boundary layer meteorology, turbulent kinetic energy,

411 cloud and precipitation (Liu et al., 2016; Huang et al., 2016; Wilcox et al., 2016). The

412 sensitivity test showed that the BrC DRE strongly depended on the absorptivity and

413 BC-to-OA ratio from crop residue burning, and the volume mixing treatment could result

414 in a higher positive DRE compared to the core/shell treatment. Several uncertainties

415 remain regarding the estimated DRE in this study, due to the mixing state and

416 morphology of the particles, burning conditions, and emission inventory. Continued

417 investigation of the mixing manner and ratio, the morphology and optical properties of

418 biomass burning aerosol, and their variation during the atmospheric aging process is still

419 required.

Atmospheric
Chemistry
and Physics
Discussions

References:

Abel, S. J., Highwood, E. J., Haywood, J. M., and Stringer, M. A.: The direct radiative effect of biomass burning aerosols over southern Africa, Atmos. Chem. Phys., 5, 1999-2018,2005.

Ackerman, T. P., and Toon, O. B.: Absorption of visible radiation in atmosphere containing mixtures of absorbing and nonabsorbing particles, Appl. Optics, 20, 3661-3668,1981.

Adachi, K., Chung, S. H., and Buseck, P. R.: Shapes of soot aerosol particles and implications for their effects on climate, Journal of Geophysical Research: Atmospheres, 115,2010.

Andreae, M. O.: Climatic effects of changing atmospheric aerosol levels, World survey of climatology, 16, 347-398,1995.

Andreae, M. O., and Gelencsér, A.: Black carbon or brown carbon? The nature of light-absorbing carbonaceous aerosols, Atmos. Chem. Phys., 6, 3131-3148,2006.

Barnard, J. C., Fast, J. D., Paredes-Miranda, G., Arnott, W. P., and Laskin, A.: Technical Note: Evaluation of the WRF-Chem "Aerosol Chemical to Aerosol Optical Properties" Module using data from the MILAGRO campaign, Atmos. Chem. Phys., 10, 7325-7340, doi:10.5194/acp-10-7325-2010, 2010.

Bauer, S. E., Ault, A., and Prather, K. A.: Evaluation of aerosol mixing state classes in the GISS modelE-MATRIX climate model using single-particle mass spectrometry measurements, Journal of Geophysical Research: Atmospheres, 118, 9834-9844, doi:10.1002/jgrd.50700, 2013.

Bond, T. C.: A technology-based global inventory of black and organic carbon emissions from combustion, J. Geophys. Res., 109, doi:10.1029/2003JD003697, 2004.

Bond, T. C.: Spectral dependence of visible light absorption by carbonaceous particles emitted from coal combustion, Geophys. Res. Lett., 28, 4075-4078,2001.

Bond, T. C., Doherty, S. J., Fahey, D. W., Forster, P. M., Berntsen, T., DeAngelo, B. J., Flanner, M. G., Ghan, S., Kärcher, B., Koch, D., Kinne, S., Kondo, Y., Quinn, P. K., Sarofim, M. C., Schultz, M. G., Schulz, M., Venkataraman, C., Zhang, H., Zhang, S., Bellouin, N., Guttikunda, S. K., Hopke, P. K., Jacobson, M. Z., Kaiser, J. W., Klimont, Z., Lohmann, U., Schwarz, J. P., Shindell, D., Storelvmo, T., Warren, S. G., and Zender, C. S.: Bounding the role of black carbon in the climate system: A scientific assessment, Journal of Geophysical Research: Atmospheres, 118, 5380-5552, doi:10.1002/jgrd.50171, 2013.

Boucher, O., and Anderson, T. L.: General circulation model assessment of the sensitivity of direct climate forcing by anthropogenic sulfate aerosols to aerosol size and chemistry, Journal of Geophysical Research: Atmospheres (1984 – 2012), 100, 26117-26134,1995.

Cao, J., Zhu, C., Chow, J. C., Watson, J. G., Han, Y., Wang, G., Shen, Z., and An, Z.: Black carbon relationships with emissions and meteorology in Xi'an, China, Atmos. Res., 94, 194-202, doi:10.1016/j.atmosres.2009.05.009, 2009.

Chang, S. G., Brodzinsky, R., Gundel, L. A., and Novakov, T.: Chemical and catalytic properties of elemental carbon., Springer, 1982.

Chapman, E. G., Gustafson Jr, W. I., Easter, R. C., Barnard, J. C., Ghan, S. J., Pekour, M. S., and Fast, J. D.: Coupling aerosol-cloud-radiative processes in the WRF-Chem model: Investigating the radiative impact of elevated point sources, Atmos. Chem. Phys., 9, 945-964,2009.

Chung, C. E., Ramanathan, V., and Decremer, D.: Observationally constrained estimates of carbonaceous aerosol radiative forcing, Proceedings of the National Academy of Sciences, 109, 11624-11629, doi:10.1073/pnas.1203707109, 2012.

Dee, D. P., Uppala, S. M., Simmons, A. J., Berrisford, P., Poli, P., Kobayashi, S., Andrae, U., Balmaseda, M. A., Balsamo, G., and Bauer, P.: The ERA-Interim reanalysis: Configuration and performance of the data assimilation system, Q. J. Roy. Meteor. Soc., 137, 553-597,2011.

469   Emmons, L. K., Walters, S., Hess, P. G., Lamarque, J., Pfister, G. G., Fillmore, D., Granier, C., Guenther, A.,

470   Kinnison, D., and Laepple, T.: Description and evaluation of the Model for Ozone and Related chemical

471   Tracers, version 4 (MOZART-4), Geosci. Model Dev., 3, 43-67,2010.

472   Fast, J. D., Gustafson, W. I., Easter, R. C., Zaveri, R. A., Barnard, J. C., Chapman, E. G., Grell, G. A., and

473   Peckham, S. E.: Evolution of ozone, particulates, and aerosol direct radiative forcing in the vicinity of

474   Houston using a fully coupled meteorology-chemistry-aerosol model, J. Geophys. Res., 111,

475   doi:10.1029/2005JD006721, 2006.

476   Feichter, J., Lohmann, U., and Schult, I.: The atmospheric sulfur cycle in ECHAM-4 and its impact on the

477   shortwave radiation, Clim. Dynam., 13, 235-246,1997.

478   Feng, Y., Ramanathan, V., and Kotamarthi, V. R.: Brown carbon: a significant atmospheric absorber of solar

479   radiation? Atmos. Chem. Phys., 13, 8607-8621, doi:10.5194/acp-13-8607-2013, 2013.

480   Fu, P. Q., Kawamura, K., Chen, J., Li, J., Sun, Y. L., Liu, Y., Tachibana, E., Aggarwal, S. G., Okuzawa, K.,

481   Tanimoto, H., Kanaya, Y., and Wang, Z. F.: Diurnal variations of organic molecular tracers and stable

482   carbon isotopic composition in atmospheric aerosols over Mt. Tai in the North China Plain: an influence of

483   biomass burning, Atmos. Chem. Phys., 12, 8359-8375, doi:10.5194/acp-12-8359-2012, 2012.

484   Gao, Y., Zhao, C., Liu, X., Zhang, M., and Leung, L. R.: WRF-Chem simulations of aerosols and

485   anthropogenic aerosol radiative forcing in East Asia, Atmos. Environ., 92, 250-266,

486   doi:10.1016/j.atmosenv.2014.04.038, 2014.

487   Grell, G. A., Peckham, S. E., Schmitz, R., McKeen, S. A., Frost, G., Skamarock, W. C., and Eder, B.: Fully

488   coupled "online" chemistry within the WRF model, Atmos. Environ., 39, 6957-6975,

489   doi:10.1016/j.atmosenv.2005.04.027, 2005.

490   Gu, Y., Liou, K. N., Xue, Y., Mechoso, C. R., Li, W., and Luo, Y.: Climatic effects of different aerosol

491   types in China simulated by the UCLA general circulation model, Journal of Geophysical Research:

492   Atmospheres (1984–2012), 111,2006.

493   Hays, M. D., Fine, P. M., Geron, C. D., Kleeman, M. J., and Gullett, B. K.: Open burning of agricultural

494   biomass: Physical and chemical properties of particle-phase emissions, Atmos. Environ., 39, 6747-6764,

495   doi:10.1016/j.atmosenv.2005.07.072, 2005.

496   Heald, C. L., Ridley, D. A., Kroll, J. H., Barrett, S. R. H., Cady-Pereira, K. E., Alvarado, M. J., and Holmes,

497   C. D.: Contrasting the direct radiative effect and direct radiative forcing of aerosols, Atmos. Chem. Phys., 14,

498   5513-5527, doi:10.5194/acp-14-5513-2014, 2014.

499   Hobbs, P. V., Reid, J. S., Kotchenruther, R. A., Ferek, R. J., and Weiss, R.: Direct radiative forcing by

500   smoke from biomass burning, Science, 275, 1777-1778,1997.

501   Hodzic, A., Jimenez, J. L., Madronich, S., Canagaratna, M. R., DeCarlo, P. F., Kleinman, L., and Fast, J.:

502   Modeling organic aerosols in a megacity: potential contribution of semi-volatile and intermediate volatility

503   primary organic compounds to secondary organic aerosol formation, Atmos. Chem. Phys., 10, 5491-5514,

504   doi:10.5194/acp-10-5491-2010, 2010.

505   Hong, S., and Dudhia, J.: 17.3 Testing of a new nonlocal boundary layer vertical diffusion scheme in

506   numerical weather prediction applications,2003.

507   Hsu, N. C., Tsay, S., King, M. D., and Herman, J. R.: Deep blue retrievals of Asian aerosol properties during

508   ACE-Asia, Geoscience and Remote Sensing, IEEE Transactions on, 44, 3180-3195,2006.

509   Huang, X., Ding, A., Liu, L., Liu, Q., Ding, K., Niu, X., Nie, W., Xu, Z., Chi, X., Wang, M., Sun, J., Guo,

510   W., and Fu, C.: Effects of aerosol–radiation interaction on precipitation during biomass-burning season in

511   East China, Atmos. Chem. Phys., 16, 10063-10082, doi:10.5194/acp-16-10063-2016, 2016.

512   Huang, X., Song, Y., Zhao, C., Cai, X., Zhang, H., and Zhu, T.: Direct radiative effect by multicomponent

Atmospheric
Chemistry
and Physics
Discussions

Open Access

EGU

513   aerosol over China, J. Climate, doi:10.1175/JCLI-D-14-00365.1, 2015.

514   Jacobson, M. Z.: A physically‐based treatment of elemental carbon optics: Implications for global direct

515   forcing of aerosols, Geophys. Res. Lett., 27, 217-220,2000.

516   Jacobson, M. Z.: Effects of biomass burning on climate, accounting for heat and moisture fluxes, black and

517   brown carbon, and cloud absorption effects, Journal of Geophysical Research: Atmospheres, 119,

518   8980-9002, doi:10.1002/2014JD021861, 2014.

519   Jacobson, M. Z.: Isolating nitrated and aromatic aerosols and nitrated aromatic gases as sources of

520   ultraviolet light absorption, Journal of Geophysical Research: Atmospheres, 104, 3527-3542,1999.

521   Jacobson, M. Z.: Strong radiative heating due to the mixing state of black carbon in atmospheric aerosols,

522   Nature, 409, 695-697,2001.

523   Kirchstetter, T. W., Novakov, T., and Hobbs, P. V.: Evidence that the spectral dependence of light

524   absorption by aerosols is affected by organic carbon, Journal of Geophysical Research: Atmospheres, 109,

525   n/a-n/a, doi:10.1029/2004JD004999, 2004.

526   Knote, C., Hodzic, A., Jimenez, J. L., Volkamer, R., Orlando, J. J., Baidar, S., Brioude, J., Fast, J., Gentner,

527   D. R., and Goldstein, A. H.: Simulation of semi-explicit mechanisms of SOA formation from glyoxal in

528   aerosol in a 3-D model, Atmos. Chem. Phys., 14, 6213-6239,2014.

529   Kodros, J. K., Cucinotta, R., Ridley, D. A., Wiedinmyer, C., and Pierce, J. R.: The aerosol radiative effects

530   of uncontrolled combustion of domestic waste, Atmos. Chem. Phys., 16, 6771-6784,

531   doi:10.5194/acp-16-6771-2016, 2016.

532   Kodros, J. K., Scott, C. E., Farina, S. C., Lee, Y. H., L'Orange, C., Volckens, J., and Pierce, J. R.:

533   Uncertainties in global aerosols and climate effects due to biofuel emissions, Atmos. Chem. Phys., 15,

534   8577-8596, doi:10.5194/acp-15-8577-2015, 2015.

535   Lack, D. A., Langridge, J. M., Bahreini, R., Cappa, C. D., Middlebrook, A. M., and Schwarz, J. P.: Brown

536   carbon and internal mixing in biomass burning particles, Proceedings of the National Academy of Sciences,

537   109, 14802-14807, doi:10.1073/pnas.1206575109, 2012.

538   Laskin, A., Laskin, J., and Nizkorodov, S. A.: Chemistry of Atmospheric Brown Carbon, Chem. Rev., 115,

539   4335-4382, doi:10.1021/cr5006167, 2015.

540   Li, J., Song, Y., Mao, Y., Mao, Z., Wu, Y., Li, M., Huang, X., He, Q., and Hu, M.: Chemical characteristics

541   and source apportionment of PM2.5 during the harvest season in eastern China's agricultural regions, Atmos.

542   Environ., 92, 442-448, doi:10.1016/j.atmosenv.2014.04.058, 2014.

543   Li, K., Liao, H., Mao, Y., and Ridley, D. A.: Source sector and region contributions to concentration and

544   direct radiative forcing of black carbon in China, Atmos. Environ., 124, 351-366,

545   doi:10.1016/j.atmosenv.2015.06.014, 2016.

546   Li, M., Zhang, Q., Kurokawa, J., Woo, J. H., He, K. B., Lu, Z., Ohara, T., Song, Y., Sreets, D. G., and

547   Carmichael, G. R.: MIX: a mosaic Asian anthropogenic emission inventory for the MICS-Asia and the

548   HTAP projects, Atmos. Phys. Chem. Discuss., submitted,2015.

549   Li, X., Wang, S., Duan, L., Hao, J., Li, C., Chen, Y., and Yang, L.: Particulate and Trace Gas Emissions

550   from Open Burning of Wheat Straw and Corn Stover in China, Environ. Sci. Technol., 41, 6052-6058,

551   doi:10.1021/es0705137, 2007.

552   Lin, G., Penner, J. E., Flanner, M. G., Sillman, S., Xu, L., and Zhou, C.: Radiative forcing of organic aerosol

553   in the atmosphere and on snow: Effects of SOA and brown carbon, Journal of Geophysical Research:

554   Atmospheres, 119, 7453-7476, doi:10.1002/2013JD021186, 2014.

555   Liu, J., Bergin, M., Guo, H., King, L., Kotra, N., Edgerton, E., and Weber, R. J.: Size-resolved

556   measurements of brown carbon in water and methanol extracts and estimates of their contribution to ambient

Atmospheric
Chemistry
and Physics
Discussions

Open Access

EGU

557   fine-particle light absorption, Atmos. Chem. Phys., 13, 12389-12404, doi:10.5194/acp-13-12389-2013,
558   2013.
559   Liu, L., Huang, X., Ding, A., and Fu, C.: Dust-induced radiative feedbacks in north China: A dust storm
560   episode   modeling   study   using   WRF-Chem,   Atmos.   Environ.,   129,   43-54,
561   doi:10.1016/j.atmosenv.2016.01.019, 2016.
562   Liu, M., Song, Y., Yao, H., Kang, Y., Li, M., Huang, X., and Hu, M.: Estimating emissions from
563   agricultural fires in the North China Plain based on MODIS fire radiative power, Atmos. Environ., 112,
564   326-334, doi:10.1016/j.atmosenv.2015.04.058, 2015.
565   Lu, Z., Zhang, Q., and Streets, D. G.: Sulfur dioxide and primary carbonaceous aerosol emissions in China
566   and India, 1996–2010, Atmos. Chem. Phys., 11, 9839-9864,2011.
567   Mlawer, E. J., Taubman, S. J., Brown, P. D., Iacono, M. J., and Clough, S. A.: Radiative transfer for
568   inhomogeneous atmospheres: RRTM, a validated correlated‐k model for the longwave, Journal of
569   Geophysical Research: Atmospheres (1984–2012), 102, 16663-16682,1997.
570   Myhre, G., Berglen, T. F., Johnsrud, M., Hoyle, C. R., Berntsen, T. K., Christopher, S. A., Fahey, D. W.,
571   Isaksen, I. S., Jones, T. A., and Kahn, R. A.: Modelled radiative forcing of the direct aerosol effect with
572   multi-observation evaluation, Atmos. Chem. Phys, 9, 1365-1392,2009.
573   Myhre, G., Samset, B. H., Schulz, M., Balkanski, Y., Bauer, S., Berntsen, T. K., Bian, H., Bellouin, N., Chin,
574   M., Diehl, T., Easter, R. C., Feichter, J., Ghan, S. J., Hauglustaine, D., Iversen, T., Kinne, S., Kirkevåg, A.,
575   Lamarque, J. F., Lin, G., Liu, X., Lund, M. T., Luo, G., Ma, X., van Noije, T., Penner, J. E., Rasch, P. J.,
576   Ruiz, A., Seland, Ø., Skeie, R. B., Stier, P., Takemura, T., Tsigaridis, K., Wang, P., Wang, Z., Xu, L., Yu,
577   H., Yu, F., Yoon, J. H., Zhang, K., Zhang, H., and Zhou, C.: Radiative forcing of the direct aerosol effect
578   from AeroCom Phase II simulations, Atmos. Chem. Phys., 13, 1853-1877, doi:10.5194/acp-13-1853-2013,
579   2013.
580   Nordmann, S., Cheng, Y. F., Carmichael, G. R., Yu, M., Denier Van Der Gon, H. A. C., Zhang, Q., Saide, P.
581   E., Pöschl, U., Su, H., Birmili, W., and Wiedensohler, A.: Atmospheric black carbon and warming effects
582   influenced by the source and absorption enhancement in central Europe, Atmos. Chem. Phys., 14,
583   12683-12699, doi:10.5194/acp-14-12683-2014, 2014.
584   Park, R. J., Kim, M. J., Jeong, J. I., Youn, D., and Kim, S.: A contribution of brown carbon aerosol to the
585   aerosol light absorption and its radiative forcing in East Asia, Atmos. Environ., 44, 1414-1421,
586   doi:10.1016/j.atmosenv.2010.01.042, 2010.
587   Peng, J., Hu, M., Guo, S., Du, Z., Zheng, J., Shang, D., Levy Zamora, M., Zeng, L., Shao, M., Wu, Y.,
588   Zheng, J., Wang, Y., Glen, C. R., Collins, D. R., Molina, M. J., and Zhang, R.: Markedly enhanced
589   absorption and direct radiative forcing of black carbon under polluted urban environments, Proceedings of
590   the National Academy of Sciences, 113, 4266-4271, doi:10.1073/pnas.1602310113, 2016.
591   Ramanathan, V., and Carmichael, G.: Global and regional climate changes due to black carbon, Nat. Geosci.,
592   1, 221-227, doi:10.1038/ngeo156, 2008.
593   Roy, D. P., Boschetti, L., Justice, C. O., and Ju, J.: The collection 5 MODIS burned area product—Global
594   evaluation by comparison with the MODIS active fire product, Remote Sens. Environ., 112,
595   3690-3707,2008.
596   Saleh, R., Marks, M., Heo, J., Adams, P. J., Donahue, N. M., and Robinson, A. L.: Contribution of brown
597   carbon and lensing to the direct radiative effect of carbonaceous aerosols from biomass and biofuel burning
598   emissions, Journal of Geophysical Research: Atmospheres, n/a-n/a, doi:10.1002/2015JD023697-T, 2015.
599   Saleh, R., Robinson, E. S., Tkacik, D. S., Ahern, A. T., Liu, S., Aiken, A. C., Sullivan, R. C., Presto, A. A.,
600   Dubey, M. K., Yokelson, R. J., Donahue, N. M., and Robinson, A. L.: Brownness of organics in aerosols

Atmospheric
Chemistry
and Physics
Discussions

Open Access

601   from biomass burning linked to their black carbon content, Nat. Geosci., 7, 647-650, doi:10.1038/ngeo2220,
602   2014.

603   Schulz, M., Textor, C., Kinne, S., Balkanski, Y., Bauer, S., Berntsen, T., Berglen, T., Boucher, O., Dentener,
604   F., and Guibert, S.: Radiative forcing by aerosols as derived from the AeroCom present-day and
605   pre-industrial simulations, Atmos. Chem. Phys., 6, 5225-5246,2006.

606   Schwarz, J. P., Gao, R. S., Spackman, J. R., Watts, L. A., Thomson, D. S., Fahey, D. W., Ryerson, T. B.,
607   Peischl, J., Holloway, J. S., Trainer, M., Frost, G. J., Baynard, T., Lack, D. A., de Gouw, J. A., Warneke, C.,
608   and Del Negro, L. A.: Measurement of the mixing state, mass, and optical size of individual black carbon
609   particles in urban and biomass burning emissions, Geophys. Res. Lett., 35, doi:10.1029/2008GL033968,
610   2008.

611   Stocker, T. F.: Climate change 2013: the physical science basis: Working Group I contribution to the Fifth
612   assessment report of the Intergovernmental Panel on Climate Change, Cambridge University Press, 2014.

613   Wang, Q., Huang, R., Cao, J., Han, Y., Wang, G., Li, G., Wang, Y., Dai, W., Zhang, R., and Zhou, Y.:
614   Mixing state of black carbon aerosol in a heavily polluted urban area of China: Implications for light
615   absorption enhancement, Aerosol Sci. Tech., 48, 689-697,2014.

616   Wang, X., Heald, C. L., Ridley, D. A., Schwarz, J. P., Spackman, J. R., Perring, A. E., Coe, H., Liu, D., and
617   Clarke, A. D.: Exploiting simultaneous observational constraints on mass and absorption to estimate the
618   global direct radiative forcing of black carbon and brown carbon, Atmos. Chem. Phys., 14, 10989-11010,
619   doi:10.5194/acp-14-10989-2014, 2014.

620   Wilcox, E. M., Thomas, R. M., Praveen, P. S., Pistone, K., Bender, F. A. M., and Ramanathan, V.: Black
621   carbon solar absorption suppresses turbulence in the atmospheric boundary layer, Proceedings of the
622   National Academy of Sciences, 113, 11794-11799, doi:10.1073/pnas.1525746113, 2016.

623   Xia, X., Li, Z., Holben, B., Wang, P., Eck, T., Chen, H., Cribb, M., and Zhao, Y.: Aerosol optical properties
624   and radiative effects in the Yangtze Delta region of China, J. Geophys. Res., 112,
625   doi:10.1029/2007JD008859, 2007.

626   Yamaji, K., Li, J., Uno, I., Kanaya, Y., Irie, H., Takigawa, M., Komazaki, Y., Pochanart, P., Liu, Y.,
627   Tanimoto, H., Ohara, T., Yan, X., Wang, Z., and Akimoto, H.: Impact of open crop residual burning on air
628   quality over Central Eastern China during the Mount Tai Experiment 2006 (MTX2006), Atmos. Chem.
629   Phys., 10, 7353-7368, doi:10.5194/acp-10-7353-2010, 2010.

630   Yang, S., He, H., Lu, S., Chen, D., and Zhu, J.: Quantification of crop residue burning in the field and its
631   influence on ambient air quality in Suqian, China, Atmos. Environ., 42, 1961-1969,
632   doi:10.1016/j.atmosenv.2007.12.007, 2008.

633   Yoon, S., and Kim, J.: Influences of relative humidity on aerosol optical properties and aerosol radiative
634   forcing during ACE-Asia, Atmos. Environ., 40, 4328-4338,2006.

635   Zaveri, R. A., Easter, R. C., Fast, J. D., and Peters, L. K.: Model for Simulating Aerosol Interactions and
636   Chemistry (MOSAIC), J. Geophys. Res., 113, doi:10.1029/2007JD008782, 2008.

637   Zhang, H., YE, X., CHENG, T., CHEN, J., YANG, X., WANG, L., and ZHANG, R.: A laboratory study of
638   agricultural crop residue combustion in China: Emission factors and emission inventory, Atmos. Environ.,
639   42, 8432-8441, doi:10.1016/j.atmosenv.2008.08.015, 2008.

640   Zhang, X., Lin, Y., Surratt, J. D., and Weber, R. J.: Sources, composition and absorption Ångstrom exponent
641   of light-absorbing organic components in aerosol extracts from the Los Angeles Basin, Environ. Sci.
642   Technol., 47, 3685-3693,2013.

643   Zhao, C., Ruby Leung, L., Easter, R., Hand, J., and Avise, J.: Characterization of speciated aerosol direct
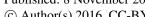644   radiative forcing over California, Journal of Geophysical Research: Atmospheres, 118, 2372-2388,

Atmospheric
Chemistry
and Physics
Discussions

Open Access

EGU

645 doi:10.1029/2012JD018364, 2013.

646 Zhuang, B., Jiang, F., Wang, T., Li, S., and Zhu, B.: Investigation on the direct radiative effect of fossil fuel

647 black-carbon aerosol over China, Theor. Appl. Climatol., 104, 301-312,2011.

648

649 **Table Captions**

650 Table 1. WRF-Chem configuration options and settings.

651 Table 2. Descriptions of the parallel simulations.

652 Table 3. Statistical analyses of the simulated meteorological variables versus the

653 ground observations. MB, mean bias; RMSE, root-mean-square error; FB, fractional

654 bias; FE, fractional error; IOA, index of agreement.

655 Table 4. The DRE differences (W m^{-2}) between the cases at TOA during the summer

656 harvest (1–21 June) in 2013.

657 Table 5. The mass concentration contributions and normalized DRE of carbonaceous

658 aerosols from crop residue burning, and the DRE of OA from crop residue burning

659 due to absorption and scattering during the summer harvest (1–21 June) in 2013.

660

661   Table 1. WRF-Chem configuration options and settings

Configuration options	
Radiation	RRTMG short- and longwave
Cumulus parameterization	New Grell Scheme (G3)
Land surface	Noah
Microphysics	Lin et al.
Photolysis	Fast-J
Gas chemistry	MOZART-4
Aerosol chemistry	MOSAIC
Boundary layer	Yonsei University
Domain settings	
Horizontal grid	52×60 (coarse) ; 49×64 (fine)
Grid spacing	75 km×75 km (coarse); 25 km×25 km (fine)
Vertical layers	25
Projection	Lambert conformal conic

662

Atmospheric
Chemistry
and Physics
Discussions

Open Access

EGU

663   Table 2. Descriptions of the main simulations.

Simulation	Emission inventory	BC-to-OC ratio	OA absorptivity	Mixing state
BASE	Comprehensive	0.27	Saleh et al. (2014)	Shell/Core
NOCB	All without crop residue burning emissions	0.27	Saleh et al. (2014)	Shell/Core
NOBCCB	All without the BC emission from crop residue burning	0.27	Saleh et al. (2014)	Shell/Core
NOOACB	All without the OA emission from crop residue burning	0.27	Saleh et al. (2014)	Shell/Core
NOBRC	Comprehensive	0.27	None	Shell/Core

Atmospheric
Chemistry
and Physics
Discussions

Open Access

664   Table 3. Statistical analyses of the simulated meteorological variables versus the

665   ground observations. MB, mean bias; RMSE, root-mean-square error; FB, fractional

666   bias; FE, fractional error; IOA, index of agreement.

Index	MB[a]	RMSE[b]	FB[c]	FE[d]	IOA[e]
2-m temperature (℃)	0.26	2.72	0.01	0.09	0.92
2-m relative humidity (%)	–0.69	13.93	–0.02	0.16	0.87
10-m wind speed (m/s)	0.99	2.01	0.45	0.65	0.61
10-m wind direction (°)	7.32	56.03			

667   [a] $MB = \dfrac{1}{N}\sum_{1}^{N}(sim - obs)$

668   [b] $RMSE = \sqrt{\sum_{1}^{N}(sim - obs)^2 / N}$

669   [c] $FB = 2\sqrt{(sim_i - obs_i)/(sim_i + obs_i)} / N$

670   [d] $FE = \sqrt{|sim_i - obs_i| / (sim_i + obs_i)^2} / N$

671   [e] $IOA = 1 - \dfrac{N \times RMSE^2}{\sum_{i=1}^{N}(|obs_i - \overline{obs}| + |sim_i - \overline{obs}|)^2}$, where the term sim and obs refer to the

672   simulated and observed meteorological values, respectively and N represents the

673   number of data pairs

674   Table 4. The DRE differences (W m^{-2}) between the cases at TOA during the summer

675   harvest (1–21 June) in 2013.

BASE−NOCB	BASE−NOBCCB	BASE−NOOACB	BASE−NOBRC
+0.39 W m^{-2}	+1.05 W m^{-2}	–0.25 W m^{-2}	+2.79 W m^{-2}

Atmospheric
Chemistry
and Physics
Discussions

Open Access

EGU

676 Table 5. The mass concentration contributions and normalized DRE of carbonaceous aerosols

677 from crop residue burning, and the DRE of OA from crop residue burning due to absorption

678 and scattering during the summer harvest (1–21 June) in 2013.

Mass concentration contributions from crop residue burning (%)[a]		Normalized DRE (W g^{-1})[b]		crop residue burning OA DRE (W m^{-2})	
BC	OA	BC	OA	absorption [c]	scattering [d]
13.5	30.3	+1109.72	−57.17	+0.85	−1.1

679 [a] The differences of BC or OA mass concentrations at surface between BASE and NOBCCB

680 or NOOACB divided by the corresponding BC or OA mass concentration at surface in BASE

681 simulation, respectively.

682 [b] The DRE of the crop residue burning sourced BC or OA (by subtracting the TOA shortwave

683 flux of NOBCCB or NOOACB from that of BASE, respectively) divided by the

684 corresponding crop residue burning sourced BC or OA mass column burden.

685 [c] By multiplying the total OA DRE due to absorption (BASE−NOBRC) with the mass

686 concentration contribution of OA from crop residue burning.

687 [d] The DRE of OA from crop residue burning (BASE−NOOACB) minus the part due to

688 absorption.

Atmospheric
Chemistry
and Physics
Discussions

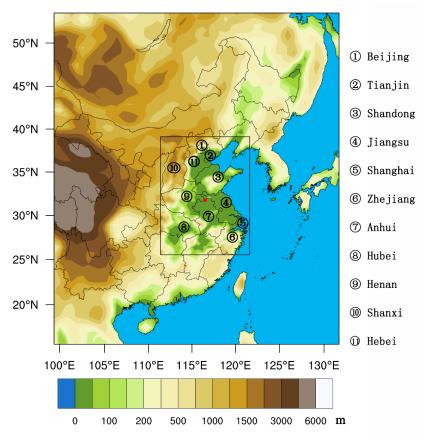Open Access

689 Figure Captions

690 Figure 1. Double-nested Weather Research and Forecasting Model (WRF) modeling

691 domains and topographic field (m); the sampling site (Suixi) is indicated by the red
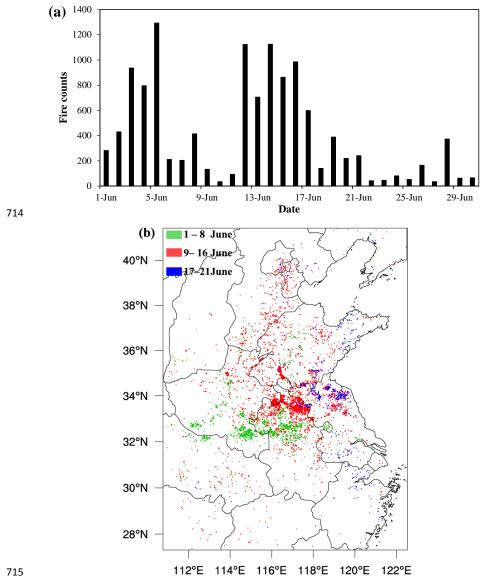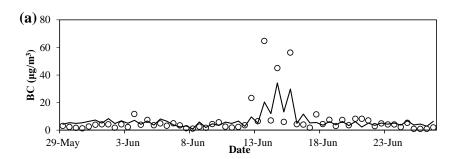
692 dot.

693 Figure 2. (a) Time series of the fire counts detected by Moderate Resolution Imaging

694 Spectroradiometer (MODIS) in East China in June 2013. (b) Spatial distribution of

695 MODIS agricultural fire counts in East China in June 2013. The green, red and blue

696 dots represent the location of fire counts detected in 1–8 June, 9–16 June and 17–21

697 June, respectively.

698 Figure 3. Time series of the observed (dots) and simulated (line) (a) black carbon (BC)

699 and (b) organic carbon (OC) mass concentrations (μg m^{-3}) at the Suixi site.

700 Figure 4. Spatial distributions of (a) carbonaceous aerosols mass concentration (μg/m^3)

701 and (b) its contribution from crop residue burning (%) in the three typical hours (6:00)

702 during the summer harvest in June 2013.

703 Figure 5. Spatial distribution of mean (a) 550-nm aerosol optical depth observations

704 from MODIS, (b) 550-nm aerosol optical depth from WRF-Chem, (c) mean

705 absorption aerosol optical depth from WRF-Chem and (d) mean carbonaceous

706 aerosols concentration (μg m^{-3}) during the summer harvest. BASE run is shown.

707 Figure 6. Spatial distribution of (a) BC direct radiative effect (DRE) and (b) brown

708 carbon (BrC) DRE due to absorption from WRF-Chem during the summer harvest.

709

Atmospheric
Chemistry
and Physics
Discussions

Figure 1. Double-nested Weather Research and Forecasting Model (WRF) modeling domains and topographic field (m); the sampling site (Suixi) is indicated by the red dot.

34

Atmospheric
Chemistry
and Physics
Discussions

Open Access

EGU

714

715

716 Figure 2. (a) Time series of the fire counts detected by Moderate Resolution Imaging

717 Spectroradiometer (MODIS) in East China in June 2013. (b) Spatial distribution of

718 MODIS agricultural fire counts in East China in June 2013. The green, red and blue

719 dots represent the location of fire counts detected in 1–8 June, 9–16 June and 17–21
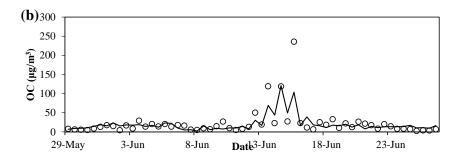
720 June, respectively.

Atmospheric
Chemistry
and Physics
Discussions

Open Access

EGU

721

722

Figure 3. Time series of the observed (dots) and simulated (line) (a) black carbon (BC)

and (b) organic carbon (OC) mass concentrations ($\mu g\ m^{-3}$) at the Suixi site.

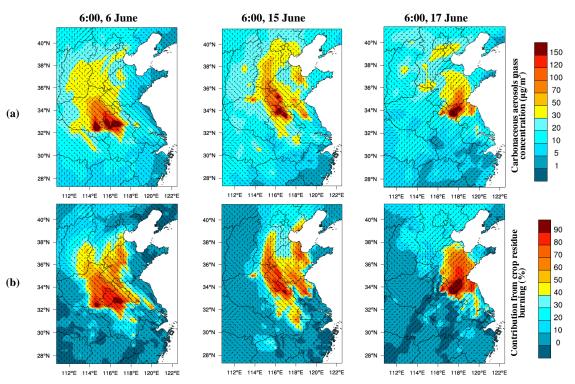Atmospheric
Chemistry
and Physics
Discussions

725   Figure 4. Spatial distributions of (a) carbonaceous aerosols mass concentration (μg/m³) and (b) its contribution from crop residue burning

726   (%) in the three typical hours (6:00) during the summer harvest in June 2013.

Atmospheric
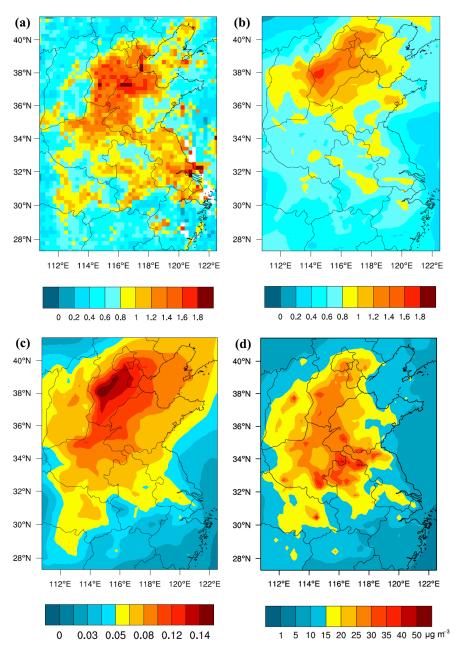Chemistry
and Physics
Discussions

Open Access

EGU

Figure 5. Spatial distribution of mean (a) 550-nm aerosol optical depth observations from MODIS, (b) 550-nm aerosol optical depth from WRF-Chem, (c) mean absorption aerosol optical depth from WRF-Chem and (d) mean carbonaceous aerosols concentration ($\mu g\ m^{-3}$) during the summer harvest. BASE run is shown.
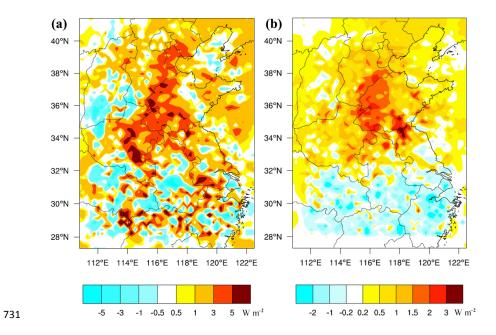
731

732   Figure 6. Spatial distribution of (a) BC direct radiative effect (DRE) and (b) brown

733   carbon (BrC) DRE due to absorption from WRF-Chem during the summer harvest.